A. Fuentes, G. Legros, A. Claverie, P. Joulain, J.P. Vantelon, J.L. Torero, *Interactions between Soot and CH^* in a Laminar Boundary Layer Type Diffusion Flame in Microgravity*, Proc. Comb. Inst. 31 (2007) 2685–2692.

Interactions between soot and CH^* in a laminar boundary layer type diffusion flame in microgravity

A. Fuentes [a,*], G. Legros [b], A. Claverie [a], P. Joulain [a], J.-P. Vantelon [a] and J.L. Torero [c]

[a] *Laboratoire de Combustion et de Détonique, 1 Av. Clément Ader, BP 40109, 86961 Futuroscope Cedex, France*

[b] *Laboratoire de Mécanique Physique, Université Paris VI, 2 Place de la Gare de Ceinture, 78230 Saint Cyr l'Ecole, France*

[c] *School of Engineering and Electronics, The University of Edinburgh, Edinburgh EH9 3JL, UK*

*Corresponding author:

Andrés Fuentes
Laboratoire de Combustion et de Détonique, 1 Av. Clément Ader, BP 40109
86961 Chasseneuil-Futuroscope Cedex, FRANCE
Fax: +33 5 49 49 82 91
E–mail: andres.fuentes@lcd.ensma.fr

Estimate of total length	=	5800
Method of determination	:	LaTeXusers
Main text	=	3650
Acknowledgments	=	50
References	=	450
Fig. 1	=	150
Fig. 2	=	250
Fig. 3	=	300
Fig. 4	=	300
Fig. 5	=	650

Abstract

A three-dimensional laminar non-buoyant diffusion flame was studied with the objective of improving the understanding of the soot production. The flame originated from a porous ethylene burner discharging into a laminar boundary layer. Soot volume fractions were measured using Laser-Induced Incandescence (LII) and the spontaneous emission from CH^* was determined using chemiluminescence. The main parameter varied was the oxidizer flow. CH^* measurements allowed to identify the reaction zone, while LII measurements permitted the tracking of soot. It was observed that soot volume fractions are inversely proportional to the global residence time. This is in contradiction to previous studies on axi-symmetric non-buoyant diffusion flames. The combined measurements allowed to establish that the apparently contradictory behaviour can be explained by an analysis of the influence of the flow field on the ratio of soot production to oxidation.

Key words: Soot, CH^*, Diffusion Flame, Laser-Induced Incandescence, Microgravity

1 Introduction

In microgravity, due to the absence of natural convection, time scales associated with combustion processes are much longer and radiation can be the predominant mode of heat transfer even for small diffusion flames [1,2]. Thus, a better understanding of soot production and radiative emissions for microgravity diffusion flames is of extreme importance to many practical combustion applications such as spacecraft fire safety [1,3,4]. Several studies have attempted to describe sooting behaviour of non-buoyant diffusion flames. Notable are the studies by Faeth and coworkers [5–7] and Konsur and coworkers [2,8,9]. Underpinning these studies is the smoke-point concept and the possibility of inferring the flame radiative losses from just the oxidizer and fuel flow rates. This concept was originally proposed by Markstein and De Ris [10], for normal gravity flames and establishes that the flame quenches due to radiative heat losses at a fixed soot concentration. Flames can therefore be "closed-tip", if fuel is consumed before this critical concentration is attained, and "open-tip" when quenching occurs before total fuel consumption. Flame lengths, and consequently co-current flame spread, can then be linked to the critical soot concentration. Markstein and De Ris empirically verified this concept and alluded to the possibility of using the smoke-point as a material flammability criterion. Despite the utility of this approach, the question remains unanswered as to how the critical soot concentration for flame quenching is attained. Furthermore, for "open-tip" flames, the flame length can only be determined if soot concentrations can be tracked along the reactive zone [5]. Prediction of other relevant parameters, such as flame geometry, also requires the definition of the flame length and therefore can only be determined for "closed-tip"

flames or if local soot concentrations are available. Soot concentrations are the result of two competitive processes: soot formation and oxidation. Both processes are influenced by the oxygen concentration which is directly linked to the structure of the flow field in the proximity of the flame. In turn, the structure of the flow field is related to experimental geometry, flow fields and characteristic velocities (residence times). Many studies have observed these dependencies. A few relevant ones will be highlighted here. Studies conducted with axi-symmetric jet flames showed that the smoke point can be modified by the experimental set-up [11,12] or the global residence time [2,9]. Konsur et al. [8,9] showed that the peak soot volume fraction decreases by reducing the characteristic flow residence time while Mortazavi et al. [13] attained similar conclusions by varying characteristic velocities in non-buoyant laminar jet diffusion flames. Luminosity of diffusion flames has also been linked to soot concentrations in boundary layer diffusion flames [14,15] and to the structure of the flow field surrounding them [16]. The numerical study of Rouvreau et al. [16] is of particular importance because it established that the orientation of the flow streamlines is at the origin of the changes in luminous intensity [16]. Given that luminous intensity can be correlated to soot oxidation, these observations provide indirect evidence of the importance of the flow field on the outcome of the soot formation/oxidation competition. Legros et al. [17] extended this work and quantified the influence of the oxidizer velocity on soot concentrations right above the fuel injection area. They showed that increasing the oxidizer velocity results in enhancing soot concentration. This observation is in contradiction to earlier studies [8,9,13] because it implies decreasing soot concentration with increasing global residence times. Nevertheless, detailed analysis of the data showed that local residence times are the source of the discrepancy, which were then associated to the differences in experimental ge-

ometry. The conclusion was that global residence times are not sufficient to characterize soot concentrations and soot measurements can not be directly extrapolated between different experimental configurations.

The configuration explored in references [14] and [15] is a three-dimensional laminar diffusion flame that could be deemed as realistic for a fire in spacecraft. The soot fields for these flames are necessary to predict radiative heat transfer. This is of special importance at the trailing edge, where radiative quenching will determine the flame length and thus co-current flame spread rates [18]. Measurements on simpler geometries are not applicable, thus direct measurement for these flames are necessary. The present study reports on combined Laser-Induced Incandescence (LII) and CH^* radical chemiluminescence measurements that define three-dimensional soot fields and quenching of the flame trailing edge. The flow velocity is varied in a parametric manner to establish the effect of flow characteristics.

2 Experimental methods

2.1 Burner and surrounding conditions

Figure 1 shows a side view of an ethylene flame obtained, in microgravity conditions, by a monochrome CCD camera, providing measurements of the visible intensity. Relevant burner dimensions are shown in Fig. 2. This laminar diffusion flame is established inside a boundary layer formed over a flat plate in the presence of an oxidizer stream flowing parallel to the surface. This configuration represents an idealized, but realistic, scenario to study quenching conditions at the trailing edge of a diffusion flame. Ethylene is chosen as fuel

because its sooting behaviour is well characterized. It is injected via a mass flow controller through the porous square plate, which has a 50 x 50 mm^2 effective section of injection. The fuel velocity V_F is fixed at 5.0 mm/s. The oxidizer corresponds to a mixture of 35% O_2 and 65% N_2. This mixture was chosen since an increased O_2 partial pressure emphasizes sooting behaviour [17]. The oxidizer flow is introduced through several settling chambers and through honeycomb plates to guarantee a laminar flow. The oxidizer velocity V_{OX} can be varied between 150 mm/s and 250 mm/s.

The flame is established inside a 50 litre stainless steel combustion chamber, which has three large quartz windows for optical access. Confinement is required for safety in microgravity facilities, but all perturbations linked to confinement have been studied before, showing that the volume of the chamber is sufficient to keep the flame free from boundary effects. The pressure is kept at atmospheric value by means of a controlled mass flowmeter placed at the exhaust of the duct. Parabolic flights provide a 22 s long microgravity period, which allows reaching steady state conditions [14]. A more detailed description of the experimental apparatus can be found in Ref. [17].

2.2 Optical diagnostics

Figure 2 shows a schematic of the experimental set-up. A Nd:YAG laser beam, pulsed at 10 Hz and emitting at 266 nm, was turned into a laser sheet, using spherical and cylindrical lenses. The laser sheet forms a probe volume centred at the burner symmetry plane ($y = 0$) with an effective length of 17 cm along the x-axis and a thickness of 500 μm along the y-axis. The laser sheet is passed through the flame to heat the soot particles up to incandescence temperature.

Based on theoretical studies of Laser-Induced Incandescence [19,20], the laser energy flux threshold required to achieve LII at 266 nm is 0.03 J/cm^2. This prevents any significant influence of the excitation energy level on the soot volume fraction measurement. For the present experiments, the laser energy was of 90 mJ/pulse (5 ns Full Width at Half the Maximum). The energy profile across the laser sheet can be assumed to follow a Gaussian distribution allowing to evaluate a mean energy flux distribution in the y direction. The mean laser energy flux computed was of 0.1 J/cm^2 which is above the aforementioned threshold.

Images were collected in the direction orthogonal to the laser sheet using an intensified charge couple device (ICCD) camera, providing 16-bit black- and-white measurements on a 1023 $\times$ 480 pixel matrix. Different approaches exist for detection [21] but here the method used is based on the recommendations of Vander Wal et al. [19]. A band-pass interference filter with peak transmission wavelength at 400 nm (60 nm FWHM) was mounted in front of the ICCD camera to avoid the most common interference sources. Using a Pulse Timing Generator (PTG), the collection of LII signals started 80 ns after the laser pulse was detected by a photodiode. This delay allows discrimination of the LII signal from soot particles with respect to the Laser Induced Fluorescence (LIF) signal from Polycyclic Aromatic Hydrocarbons (PAH) [19]. Both phenomena are simultaneously induced by the 266 nm excitation but the latter has a much faster decay rate. The intensifier gate width was of 50 ns, which gives significant LII intensity levels 80 ns after the laser pulse. For these non-buoyant diffusion flames soot particle diameter is expected to be poly-dispersed therefore for these conditions the signal intensity only weakly influenced by particle diameter [19].

Another ICCD camera was devoted to CH^* chemiluminescence measurements. This camera recorded one side-view frame between each laser pulse with an intensifier gate width of 50 ns. This camera was mounted with a narrow band filter centred at 431 nm (10 nm FWHM). CH^* radicals have been proved to be central to many hydrocarbon combustion chemical pathways [22] as they originate from the reaction between O_2 and C_2H. These excited radicals return to ground-state either through collisional quenching or through spontaneous fluorescence, whose $A^2\Delta \rightarrow X^2\Pi$ transition occurs at 431.4 nm. Therefore, CH^* chemiluminescence measurements can be directly related to the burning rate of the primary fuel (e.g. ethylene here) [23].

A $f/0.95$ 17 mm focal length lens was mounted on each camera focused at the burner plane of symmetry. The spatial resolution of the LII and CH^* images were determined by the pixel size in the ICCD matrix and the detection optics. The overall result for both techniques in the present experiment was that each pixel corresponds to a region of 0.22 mm $\times$ 0.22 mm.

Before the calibration procedure began, the raw LII and CH^* signals were corrected for background noise. Variation in the camera dark-current intensity was the only major source of background noise, since flame luminosity, as a source of background noise, was largely removed by using narrow bandpass filters and short camera gate times.

To convert the arbitrary unit of LII signals to absolute soot volume fractions, an in situ calibration procedure was adopted by comparing the LII measurements to laser extinction measurements [20,21]. For this purpose the same flames in microgravity conditions where used duplicating the experimental conditions. The various peak soot volume fraction at different stream-wise lo-

cations where used to calibrate the LII signals. These flames are inherently three-dimensional in the quenching zone, therefore an original technique was used to evaluate the soot volume fraction at the trailing edge via light extinction measurements [17,24].

The interference signals of LII are usually caused by laser scattering, laser-induced fluorescence and flame spontaneous emission (in the visible spectrum, mainly C_2 and CH^* chemiluminescence). These signals were either blocked by the bandpass filter or avoided by the time delay of ICCD in this work.

Energy profile measurements have been carried out all along the laser plane by means of acetone PLIF. Thus, a correction for the excitation energy distribution has been applied to LII frames. Eventually, attenuation of LII signal by the flame has also been estimated based on extinction measurements [17].

However, it is recognized that there might be significant uncertainties associated with optical properties of the soot in extinction measurements, ICCD spatial response, non-monochromatic light for the extinction experiments and variation of the laser energy output. In this work these effects are considered and evaluated by the calibration procedure.

This study aims to produce a relative comparison of CH^* intensity profiles for this particular configuration [17]. As discussed by Legros et al., at a given x within the two-dimensional part of the flame (see Fig.1), the peak intensity of a CH^* profile, $I(z)$, can be assumed to result only from the emission of the flame two-dimensional region, i.e. from the integration of the CH^* chemiluminescence over the width of the burner (50 mm). Deconvolution of the CH^* signal peak would not significantly reduce errors, therefore the evolution of the peak intensity and its location along the x-coordinate can provide the sought

relative comparison for different values of V_{OX}. Comparisons of the CH^* intensity distributions with LII profiles in the symmetry plane of the burner should provide valuable information for the assessment of the interaction between soot and flame quenching.

3 Results and discussion

Figure 3 (top) represents a computed contour obtained from the LII measurements for an oxidizer velocity of $V_{OX} = 200$ mm/s and injection of ethylene fuel of $V_F = 5.0$ mm/s. The colour bar shows the soot volume fraction in ppm obtained by means of the calibration and correction procedure. Fig. 3 (bottom) exhibits profiles at different x locations of soot volume fraction as a function of the z coordinate for the same conditions. The first three cross-sections are located above the porous square (e.g. from $x \geq 0$ mm to $x \leq 60$ mm) and the others in the trailing edge zone ($x > 60$ mm). These soot volume fraction profiles show that the concentrations increase within the region of the porous square. For this flow condition, it is observed that the maximum is located between $x > 60$ mm and $x < 90$ mm and decays until almost complete disappearance at $x = 120$ mm.

A representative frame of CH^* spontaneous emission is shown in Fig. 4 (top) for the same flow conditions as above. In this case, the contour colour bar represents the relative emission obtained directly from the ICCD. Cross-sections of CH^* are plotted in Fig. 4 (bottom). These graphs present the CH^* intensity versus the z coordinate at different x locations over the plate, matching those presented for the soot profile locations. For this condition, the CH^* peak increases from the leading edge of the porous square ($x \geq 0$ mm) until reaching

a maximum located between $x \geq 40$ mm and $x \leq 70$ mm, while almost no CH^* emission can be found downstream ($x \geq 90$ mm). Therefore, for these conditions, CH^* and soot profiles follow similar tendencies. However, the CH^* profiles are located far above the soot zone, showing almost no overlap [17]. Furthermore, the CH^* peak maximum occurs upstream of the soot peak maximum and CH^* disappears earlier than soot.

Within the CH^* reactive zone soot is being produced and consumed. Eventually, the ethylene reaction will quench, in a region of high soot concentration, which is very close to the location of maximum concentration [24]. Thus, the ratio of soot production to oxidation is strongly linked to the ethylene quenching, therefore to the flame length. This is an important observation that has been discussed previously by Markstein and De Ris [10]. These authors argue that final quenching will occur at a constant soot concentration due to a decrease in flame temperature associated to radiative heat losses.

The integrated CH^* emission intensity (over the z-coordinate) was obtained across the reaction zone for all locations in the x direction. The x-axis has been normalized by the burner characteristic length, L_P. Thus, the porous square is located between 0 and 1. Figure 5(a) shows the evolution of the integrated CH* emission as a function of x/L_P for different oxidizer flows. The flow velocity does not affect the region close to the leading edge, where the integrated intensities are identical for all flow velocities and increase linearly as a function of x/L_P. In this zone the reaction increases linearly mainly due to the local fuel accumulation.

Local fuel consumption rate is controlled by the quantity of oxygen available. The oxygen supply can be established by integration over the boundary layer

thickness and thus the fuel consumption can be defined assuming stoichiometric combustion. For this flow conditions the local fuel consumption rate is far smaller than the fuel injected by the pourous burner leading to accumulation of fuel. Fuel accumulation can be easily demonstrated to be an almost linear function of x. In a regime away from quenching, where infinite chemistry can be assumed, fuel accumulation results in faster fuel supply to the reaction and thus an increase in CH^* intensity following the same trends as the local excess pyrolyzate [25].

At some point downstream, the CH^* intensity deviates from the linear trend. The deviation is symptomatic of an increased dominance of finite chemistry. This is consistent with a larger presence of soot and the subsequent reduction of flame temperature. The linear regime is extended as the flow velocity increases, emphasizing previous observations of a more robust flame as the oxidizer velocity increases [14,15]. The peak of the integrated intensity is more important when the characteristic residence time decreases and the peak move towards trailing edge.

This result is also in agreement with the observations of Legros et al. [17], that showed that an increase in the oxidizer velocity leads to an increase in the CH^* intensity in the burner zone. Also, it is possible to observe that the reaction zone is longer when oxidizer velocity increases, enhancing both soot formation and soot oxidation. Thus the frequently observed longer and more intense flames [14,15,17] appear also for the CH^*.

Eventually, flame chemistry will lead to a decay of the CH^* intensity until the ultimate disappearance of any trace of CH^*. This issue is of extreme importance because it is directly linked to the definition of the flame length, which

will inevitably imply an arbitrary definition of extinction. First, it is possible to consider that the reaction is finished when the CH^* stop to increase linearly (see Fig. 5(a)). The beginning of this decrease in the reaction rate could be used as a way to define the length of the reaction zone. The second possibility is to estimate the reaction length as the peak in the integrated intensity. After this peak the reaction is controlled by a decaying finite chemistry.

The observed features of these measurements are of great importance because they allow to establish clear and quantitative ways of defining the flame length. Methodologies such as luminous intensities, CH^*, OH^* concentrations all require the definition of an arbitrary threshold beyond which the flame is considered to be quenched.

Figure 5(a) therefore provides a definition of a characteristic length scale for the reaction zone while the identification of the peak CH^* intensity at each location in x allows to establish the stand-off distance. The stand-off distance has been normalized using the Blasius boundary layer thickness (δ) and the results are presented in Fig. 5(c) for different flow velocities. As expected, the boundary layer thickness normalizes well the stand-off distance leading to an almost constant value (Fig. 5(c)). No density correction was incorporated in the definition of the boundary layer, given that flame temperatures are unknown. The departure from a constant value could be attributed to the absence of a density correction but this issue still needs to be addressed.

Soot volume fraction measurements were integrated across the entire reactive zone for each location in x. The integrated values are presented in Fig. 5(b) as a function of x/L_P for different oxidizer flow velocities. It can be noted that the concentration increases quickly in the region above the burner

$(0 < x/L_P < 1)$. Integrated soot volume fractions reach a maximum, for the three flow velocities, approximately in the region where the abrupt diminution of the signal of CH^* begins (see Fig. 5(a)). It is important to note that the peak concentration of soot increases also with the flow velocity. These observations are all consistent with Figures 5(a) and 5(c) as well as with previous experiments that established that there is an increase in reaction intensity with the flow velocity [14,15] as well as soot concentration [17].

Once the peak has been attained, a concentration plateau is followed by decay. Both plateau and decay always occur in regions where the CH^* concentrations have already dropped significantly. It is clear that through the decay process soot is not being formed and oxidation dominates the ultimate soot concentration. The decay region is pushed downstream as the flow velocity increases. This is in contradiction with other studies on laminar, non-buoyant axi-symmetric flames [9], where soot volume fraction peaks were found to approach the fuel source as the oxidizer velocity was increased. The differences could be attributed to the differences in flow structure as well to the near quenching nature of these microgravity flames.

Another way to analyze the influence of the oxidizer velocities in soot particles is to determine the position of the peak soot volume fraction for x streamwise coordinate versus z-coordinate. This will correspond to a stand-off distance based on the soot peak location. Figure 5(d) shows the evolution of the location of the peak soot volume fraction as a function of x/L_P and for different oxidizer velocities. The three curves show the same tendency. In the first part the peak increases between 0 and 1, and the local ratio of soot-formation to soot-oxidation increases and moves towards the reaction zone. As the soot formation zone approaches the flame and the streamlines begin to penetrate this region,

oxidation increases.

For $x/L_P > 1$, the location of the peak soot concentration remains relatively stable, following the same behaviour as in the reaction zone. When quenching by CH^* appears (see Fig. 5(a) and 5(c)) soot particles are accelerated outwards. The particles are mainly impelled by the streamlines exiting from the flame. When the oxidizer velocity increases, the streamlines push the peak of soot volume fraction towards the plate.

Numerous studies have been performed on non-buoyant round laminar jet diffusion flames burning in co-flowing air [5,6,9,12]. These studies show that for the "open-tip" flames, the quenching of the reaction zone occurs before the soot particles are completely oxidized, releasing soot from the flame. Empirical relations are given to interpret and to correlate the length of the flame. The correspondence between predictions and data are remarkably good in the case of "close-tip" flames. However, these correlations show discrepancies for the "open-tip" flame. The analysis of the cases studied here shows that this particular type of flame presents the characteristics of an "open-tip" flame. The main physical mechanisms observed and described for axi-symmetric flames appear here too. Nevertheless, the different flow structure results in important differences that previously had been deemed as unexplained contradictions.

4 Conclusions

An experimental study using CH^* and LII measurements has been conducted to explain observed differences in laminar non-buoyant diffusion flames. Axi-symmetric flames show a decrease in length and soot concentration with an

increase in air co-flow. Boundary layer flames have shown the opposite trend. The present measurements show that the differences arise because of the effect that specific stream lines have in the ratio of soot production to soot oxidation. In boundary layer flames, the reaction increases in strength with an increase in the flow velocity. This results in an increase in soot production. The reaction zone also increases in length. Beyond quenching, soot continues to glow but its concentration reaches a peak and then decreases.

Acknowledgments

This work was funded by CNES and ESA. Parabolic flights campaigns took place on board the Novespace A300-ZeroG.

References

[1] S.L. Olson, J.S. T'ien, *Combust. Flame* 121 (2000) 439–452.

[2] C.M. Megaridis, B. Konsur, D.W. Griffin, *Proc. Combust. Inst.* 26 (1996) 1291–1299.

[3] A.C. Fernandez-Pello, D.C. Walther, J.L. Cordova, T. Steinhaus, J.G. Quintiere, J.L. Torero, H. Ross, *Space Forum* 6 (2000) 237–243.

[4] J.L. Torero, T. Vietoris, G. Legros, P. Joulain, *Combust. Sci. Technol.* 174 (2002) 187–203.

[5] K.C. Lin, G.M. Faeth, P.B. Sunderland, D.L. Urban, Z.G. Yuan, *Combust. Flame* 116 (1999) 415–431.

[6] K.C. Lin, G.M. Faeth, *AIAA Journal* 37 (1999) 759–765.

[7] F. Xu, Z. Dai, G.M. Faeth, *AIAA Journal* 40 (2002) 2439–2446.

[8] B. Konsur, C.M. Megaridis, D.W. Griffin; *Combust. Flame* 116 (1999) 334–347.

[9] B. Konsur, C.M. Megaridis, D.W. Griffin, *Combust. Flame* 118 (1999) 509–520.

[10] G.H. Markstein, J. De Ris, *Proc. Combust. Inst.* 20 (1984) 1083–1094.

[11] P.B. Sunderland, S. Mortazavi, G.M. Faeth, D.L. Urban, *Combust. Flame* 96 (1994) 97–103.

[12] D.L. Urban, Z.G. Yuan, P.B. Sunderland, K.-C. Lin, Z. Dai, G.M. Faeth, *Proc. Combust. Inst.* 28 (2000) 1965–1972.

[13] S. Mortazavi, P.B. Sunderland, J. Jurng, Ü.Ö. Köylü, G.M. Faeth, *AIAA paper* (1993) 93–0708 .

[14] T. Vietoris, J.L. Ellzey, P. Joulain, S.N. Mehta and J.L. Torero, *Proc. Combust. Inst.* 28 (2000) 883–2889.

[15] L. Brahmi, T. Vietoris, S. Rouvreau, P. Joulain, L. David, J.L. Torero, *AIAA Journal* 43 (2005) 1725–1733.

[16] S. Rouvreau, P. Joulain, H.Y. Wang, P. Cordeiro, J.L. Torero, *Proc. Combust. Inst.* 29 (2002) 2527–2534.

[17] G. Legros, P. Joulain, J.P. Vantelon, D. Bertheau, A. Fuentes, J.L. Torero, *Combust. Sci. Technol.* 178 (2006) In Press.

[18] S. Bhattacharjee, R. Altenkirch, *Proc. Combust. Inst.* 23 (1991) 1627–1633.

[19] R.L. Vander Wal, K.A. Jensen, M.Y. Choi *Combust. Flame* 109 (1997) 399–414.

[20] C.R. Shaddix, K. Smyth, *Combust. Flame* 107(1996) 418–452.

[21] R.J. Santoro, C.R. Shaddix, *Laser-Induced Incandescence*, in: Applied combustion diagnostics, First Edition, Taylor and Francis, London, 2003.

[22] H.N. Najm, P.H. Paul, C.J. Mueller, P.S. Wyckoff, *Comb. and Flame*, 113 (1998) 312–332.

[23] P.A. Berg, D.A. Hill, A.R. Noble, G.P. Smith,J.B. Jeffries, D.R Crosley, *Comb. and Flame*, 121 (2000) 223–235.

[24] G. Legros, A. Fuentes, P. Ben-Abdallah, J. Baillargeat, P. Joulain, J.P. Vantelon, J.L. Torero, *Opt. Lett.*, 30 (2005) 3311–3313.

[25] P.J. Pagni, T.M. Shih, *Proc. Combust. Inst.* 16 (1977) 1329–1343.

List of Figures

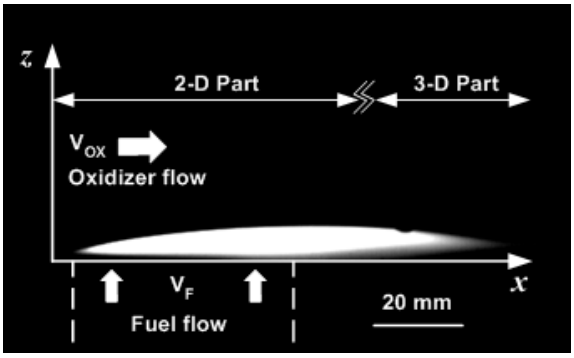

Fig. 1. Greyscale side view of the visible flame for $V_{OX} = 200$ mm/s and $V_F = 5.0$ mm/s.

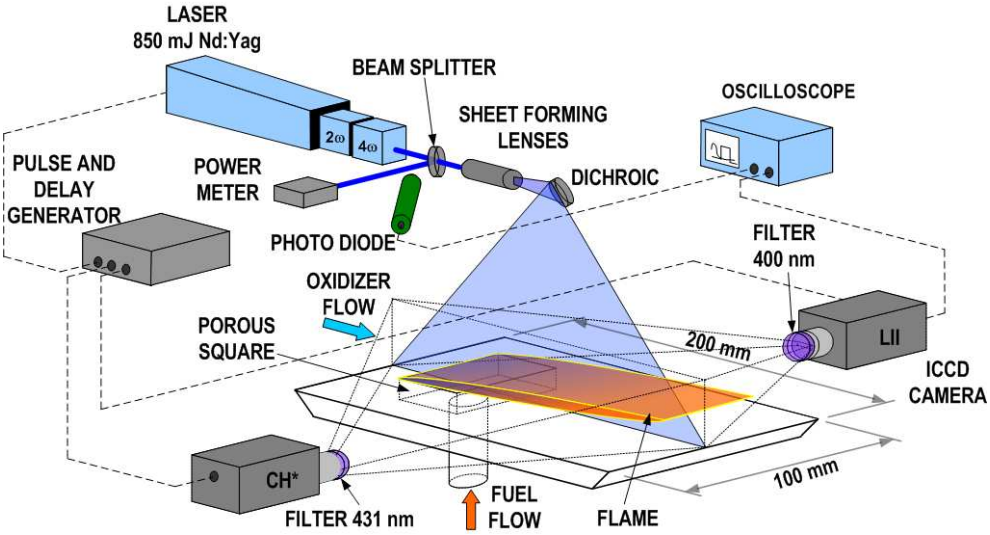

Fig. 2. Schematic of experimental apparatus.

"Color figure in electronic version only"

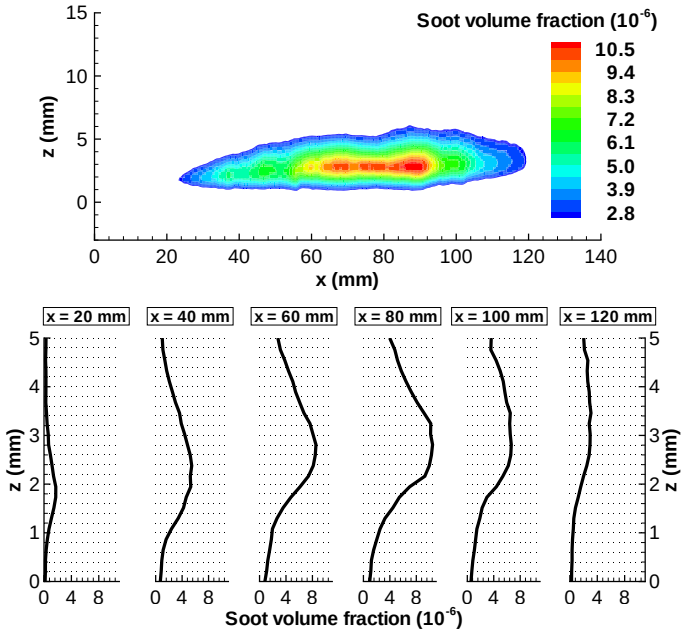

Fig. 3. Computed contours of soot volume fraction (top) and cross-sections at different x streamwise coordinate values (bottom) for $V_{OX} = 200$ mm/s and $V_F = 5.0$ mm/s.

"Color figure in electronic version only"

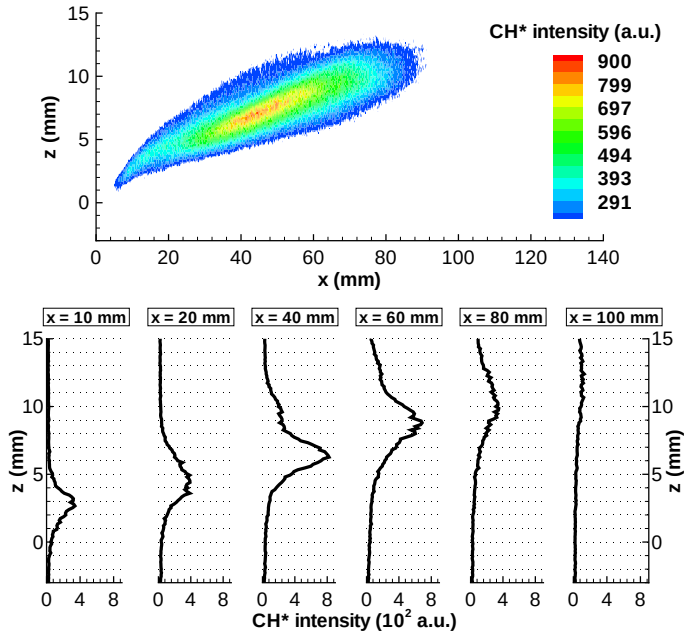

Fig. 4. Computed contours of CH* spontaneous emission (top) and cross-sections at different x streamwise coordinate values (bottom) for V_{OX} = 200 mm/s and V_F = 5.0 mm/s.

"Color figure in electronic version only"

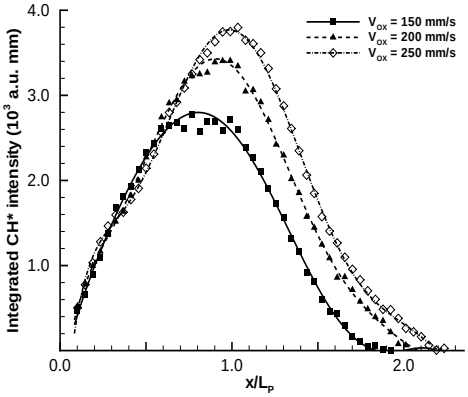

(a) Integrated CH* emission.

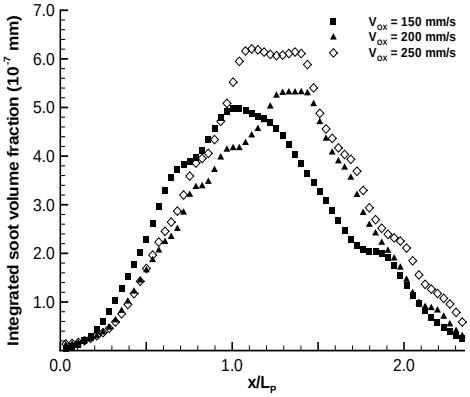

(b) Peak of integrated soot volume fraction.

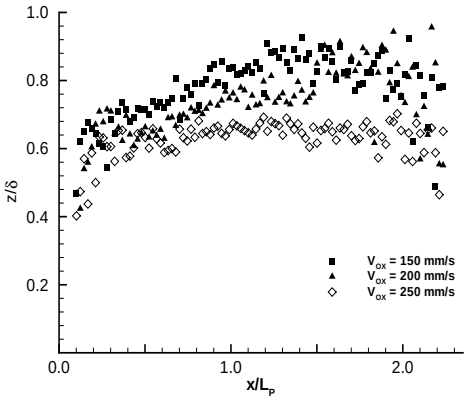

(c) CH* normalized peak position.

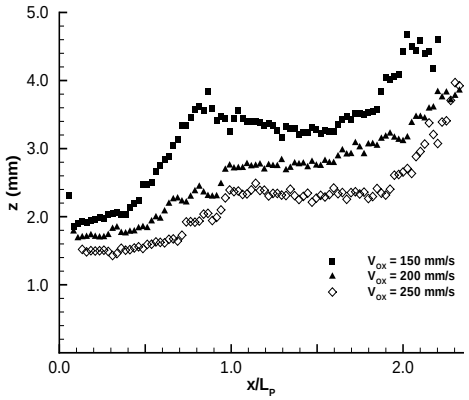

(d) Integrated soot volume fraction peak position.

Fig. 5. CH* emission and soot volume fraction profiles versus x/L_P normalized streamwise coordinate at differents oxidizer velocities. The injection fuel region (porous square) is between 0 and 1. The δ represents the boundary layer thickness